한국동력기계공학회지 제14권 제3호 pp.25~32 2010년 6월

CFD and Experimental Study of Gas Flow inside the Wounding Steel Pipe Fitted in Reciprocating Hydrogen Compressor
왕복동식 수소 압축기의 강관 관로 내부 가스흐름의 CFD와 실험

H. S. Chung, M. Sq. Rahman, G. H. Lee, J. S. Woo, B. H. Kim and H. M. Jeong
정한식 · 라흐만 · 이경환 · 우주식 · 김보한 · 정효민

(received 13 July 2009, revised 4 May 2010, accepted 7 May 2010)

주요용어 : 수소압축(Hydrogen Compression), 강관(Steel Wound Pipe), 맥동압감소(Pressure Pulsation Reduction), 압력손실(Pressure Loss), 전산유체역학(CFD)

요 약 : 전 세계적으로 급속도로 인기가 더해가고 있는 수소에너지는 높은 전환 효율성, 재생성, 친환경적인 특징을 가지며 미래의 주 에너지가 될 것이다. 왕복동식 압축기를 통과한 후의 수소 가스의 압력은 높은 맥동압을 가진다. 스너버는 압축기의 한 구성품으로 맥동압을 낮추고 수소가스의 불순물을 제거하기 위해 사용된다. 이 연구에서의 실험은 스너버 시스템에 사용된 강관의 맥동에 관해 조사하기 위해서 수행되었다. 맥동압은 12 Hz ~ 60 Hz의 모터속도에서 RMS값을 기준으로 0.1625% ~ 0.5305% 그리고 평균압력을 기준으로 0.1621% ~ 0.5277% 감소하였다. 압력손실은 RMS값을 기준으로 0.1092% ~ 1.4419%, 평균압력을 기준으로 0.1493% ~ 1.7507%로 측정되었다. CFD를 이용한 수치해석값은 실험값이 거의 비슷한 결과를 나타내고 강관 관로 내부 가스의 자세한 압력을 설명하기 위한 중요한 역할을 수행한다.

1. Introduction

Global energy requirements are mostly dependent on fossil fuels, about 80% of the present world energy demand [1]. During the last century fossil fuels became popular for their very useful properties not shared by non-conventional energy sources (such as solar). Unfortunately, fossil fuels are not renewable [2]. In addition, pollutants emitted by fossil energy systems (e.g. CO, CO_2, CnHm, SOx, NOx, radioactivity, heavy metals, ashes, etc.) are greater and more damaging than those that might be produced by a renewable based hydrogen energy system [3]. Harmful effects on environment for fossil fuel production and consumption stress scientists towards new alternative sources. The green energy based hydrogen system can be one of the best solutions for accelerating and ensuring global stability and substantiality. Therefore, the production of hydrogen from non-fossil fuel sources and the development and application of green energy technologies are becoming crucial in this century for better transition to hydrogen economy [4]. A scenario study has been reported incorporating a complete set of new technologies (including hydrogen production) to reduce CO_2 emissions by the year 2040 [5]. Hydrogen production by different approaches for splitting water have been summarized by Bockris as follows: electrolysis, plasmolysis, magnetolysis, thermal approach (direct, catalytic and cyclic decomposition of water, as well as magmalysis), use of light (photosensitized decomposition using dyes, plasma induced photolysis, photoelectrolysis, photo-aided electrolysis, the indirect path towards hydrogen by photoelectrolysis: the photo-electrochemical reduction of CO_2 and photovoltaic electrolysis), biocatalytic decomposition of water,

정효민(교신저자) : 경상대학교 정밀기계공학과, 해양산업연구소
E-mail : hmjdng@gnu.ac.kr, Tel : 055-646-4766
라흐만, 이경환, 우주식 : 경상대학교 대학원 정밀기계공학과
김보한 : 경상대학교 정밀기계공학과
정한식 : 경상대학교 정밀기계공학과, 해양산업연구소

radiolysis and other approaches [6]. The assertion of "hydrogen is considered a promising future fuel for vehicles" is based on three main arguments: the potential reducing greenhouse gases from the transport sector, greater energy supply security, i. e. hydrogen can be produced from many energy sources and hence the risk of shortage of supply may be reduced; the potential of zero local emissions with the use of fuel cells. A full scale hydrogen infrastructure with production facilities, a distribution network and refueling stations is costly to build. The venture of constructing a hydrogen refueling infrastructure constitutes long-term, capital-intensive investment with great market uncertainties for fuel cell vehicles. Therefore, reducing the financial risk is major objective of any long-term goal to build hydrogen infrastructure [7].

One of the most important processes in the hydrogen gas handling is the compressing system. This process is needed in all step of hydrogen gas energy utilization: production, storage, distribution until using [8]. In industrial application, hydrogen gas compressing system is frequently used as the transferring or storing force device. It needs to be in high pressure condition; usually reciprocating type compressor is used. There developed pressure harmful pulsation inherently due to reciprocating mechanism. Snubber can be used to turn down to a allowable limit. The single snubber is not sufficient for damping fluctuation. There needs more than one snubber. Steel pipe of specific diameter and length connect the snubbers. These pipe act as cooling chamber of temperature that develope during high pressure generation. As an essential component compressing plant it affect selection and operation of it. The efficiency of hydrogen compressing depends on wounding pip including other components. As it is not possible to measure at all points of interest by experiment, CFD simulation is used to find out pressure and its pulsation at any point even where it is very hard to measure or need high technical know-how, money and time, often give erroneous results. This research is taken to study the features of gas pressure and gas flow phenomena inside this wounding steel pipe fitted between two snubbers. Specifically, the experimental and CFD study of pressure pulsation situation inside the wounding steel pipe.

2. Methodology

2.1 Apparatus and test procedure

Four sensor holding structures for pressure measurement were made with acryl material. The curved steel pipe was attached to these sensor structures through small PVC pipe with clamp tightly. The experimental set up block diagram of the experiment is shown in Fig. 1. Three arms steel pipe properties are summaries in table 1. The setting of different parts was attached to a frame to resist vibrations. The experiment conducted by running the compressor and setting motor frequency at 12, 24, 36, 48, and 60 Hz. Pressure from two points were taken at a time. Pressure values were measured by pressure sensors amplified and recorded them using data logger in a computer.

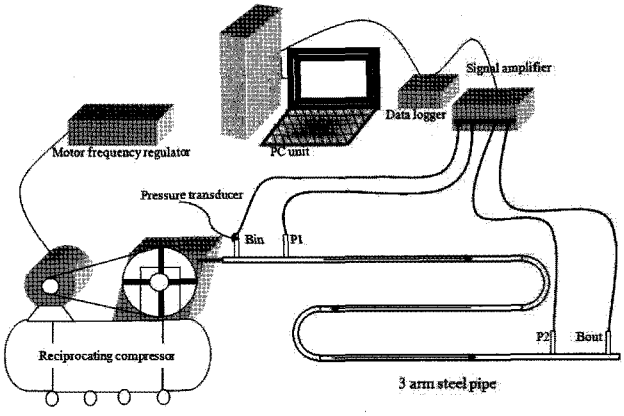

Fig. 1 Block diagram of experimental set up

Table 1 Steel pipe properties

Dimension	Value
Outer Diameter	16 mm
Thickness	1.5 mm
Bending radius	50 mm

2.2 Methods of pressure characteristics analysis

In Motor driven reciprocating pump was used in this experiment in which a variable frequency drive control its rotation. The maximum motor rotation was 1800 rpm at maximum frequency (60 Hz). Relationship between compressor frequency and motor frequency were found as in eq. 1.

$$f_{comp}\ [Hz\ ] = f_{set}\ [Hz\ ] \times 0.214 \tag{1}$$

The periodic action of propelling gas through a pipe by the to and fro movement of the piston in the cylinder in reciprocating compressor causes pulsation. The piston-crank-valve mechanism generates a variable pressure, which over time creates a composite pressure wave in the suction and discharge pipe. This composite wave is made up of a number of waves. Due to periodic wave generation, multiple frequencies of pulsation are created that causes the force of vibration in the whole system whole system.

Pressure produced by a piston in reciprocating compressor is fluctuating. Simple description of fluctuating notation is shown in Fig. 2. From this figure, pressure value and pressure amplitude can be derived as eq. (2) and (3).

$$p = \frac{p_{max} + p_{min}}{2} \tag{2}$$

$$A = \frac{p_{max} - p_{min}}{2} \tag{3}$$

Same with the other gas line utilities, gas that passing through a snubber will be reduced in pressure and reduced in pressure fluctuation. It is related to the amplitude of pressure. The pressure reduction or loss and amplitude reduction can be expressed in the percentage by the eq. (4) and (5), respectively.

$$P_{red}(\%) = \frac{P_{in} - P_{out}}{P_{in}} \times 100\,\% \tag{4}$$

$$A_{red}(\%) = \frac{A_{in} - A_{out}}{A_{in}} \times 100\,\% \tag{5}$$

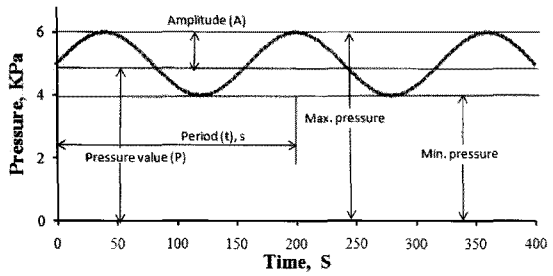

Fig. 2 Basic theory of pressure pulsation

Experimental data at every section were collected using data logger and analyzed them. RMS values of input and output of pressure were used for pressure loss. FFT analysis was done to on data to find out amplitude values of the pressure waves along the snubber. The resultant value of the variables was calculated by taking square root of summation of squares of all values [9]. Pressure loss was obtained by eq. (4) and the pressure pulsation reduction was calculated by eq. (5).

2.3 CFD Methodology

Model for simulation is made regarding the fluid passage in the steel pipe. The model was built considering the fluid area only in CATIA. The grid was generated using Pro-Surf and Pro-Am (Auto Mesh). Model was finally composed the number of 86909 trim cells (Fig. 3).

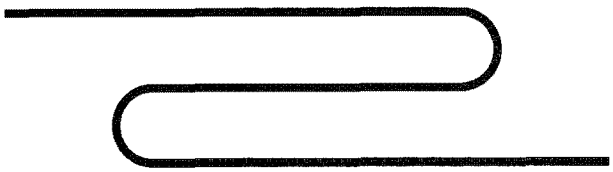

Fig. 3 Grids in steel pipe model

The CFD solver used in this study is STAR CD version 3.24. In the present study, the 3D, unsteady state, finite volume method was used. . The flow also was assumed as compressible fluid. SIMPLE (Semi Implicit Method for Pressure-Linked Equations) algorithm was employed with max residual 0.001, for linked variables. Material applied was air. For turbulence modeling, k- ε high Reynolds number model, explained in

mathematical model part, was used. Boundary conditions set in this study, accordingly data obtained from experiment at point B_{in} and point B_{out} The flow governing equations: conservation of mass, conservation of momentum and energy equations are as follows as in the Star CD 3.24 Methodology Book [10] and solutions of these equations by Star CD 3.24 software.

3. RESULTS AND DISCUSSION

Figure. 4 shows the relation between the motor frequency and compressor frequency. When motor frequency increases compressor frequency also increase. It depends upon the diameter of the motor pulley and compressor pulley. The frequency that transformed from motor to compressor were 2.14, 4.28, 6.42, 8.56, 10.7, 12.84 Hz with corresponding motor frequency 10, 20, 30, 40, 50, 60 Hz.

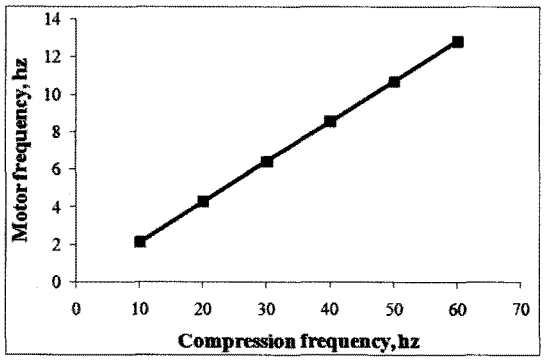

Fig. 4 Relation between motor frequency and compressor frequency

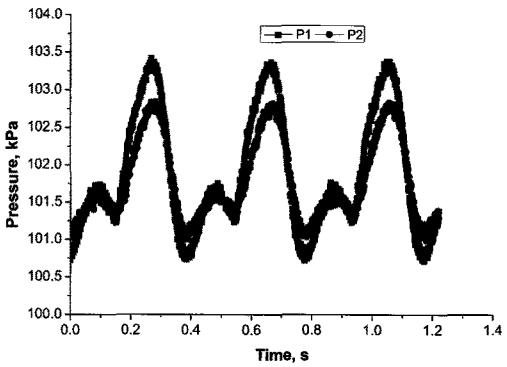

Fig. 5 Pressure wave at point 1 and point 2 for 12Hz motor speed

The motor speed 12Hz was causing pressure wave with maximum, minimum, average and RMS pressure values of 103.4183, 100.7321, 102.0752, 101.9027kPa at point 1 and 102.8410, 101.0045, 101.9228, 101.7919kPa at the end of the steel pipe. The curves had also some small peaks other than maximum and minimum peaks (Fig. 5).

The compressor generates pressure wave with 105.5359, 100.7096, 103.1227, 102.8125kPa maximum, minimum and average pressure for point 1 for 24 hz but there are a reduced of all in point 2 like 104.2107, 101.0045, 102.6076kPa, respectively, for the maximum, minimum and average pressure. The RMS values of point 1 and point are 102.4190, 102.6076kPa (Fig. 6).

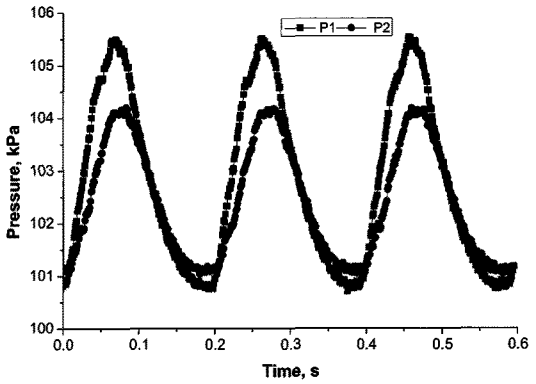

Fig. 6 Pressure wave at point 1 and point 2 for 24 Hz motor speed

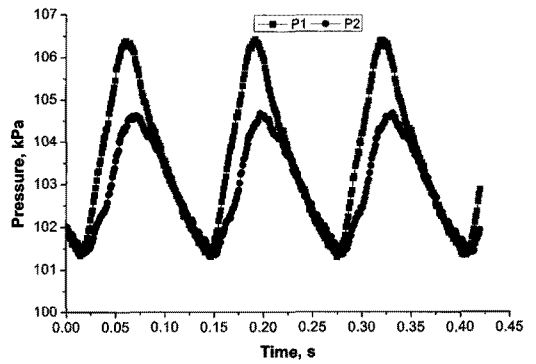

Fig. 7 Pressure wave at point 1 and point 2 for 36Hz motor speed

Fig. 7 shows the wave view of the pressure in details at point 1 and point 2 when the compressor speed was 36 Hz. The maximum peak

of pressure for point 1 and point 2 are 106.4113, 104.6775kPa and the minimum are found as 101.2932, 101.3565 kPa. The RMS values are 103.6647, 102.9897kPa for the start and end point of the steel pipe. It shows that the local peaks are illuminates as the speed of the motor was increasing.

At the 48 Hz maximum and minimum pressure in a cycle were 107.7133, 105.2743 with an average of 105.1430kPa for point 1 and for point 2 they were 105.2743, 102.3207, 103.7975kPa (Fig. 8).

The highest and lowest peak of pressure during 60Hz motor operation at two ends were 109.3445, 104.0992; 106.1237, 103.5832kPa, respectively, with some local peaks (Fig. 9).

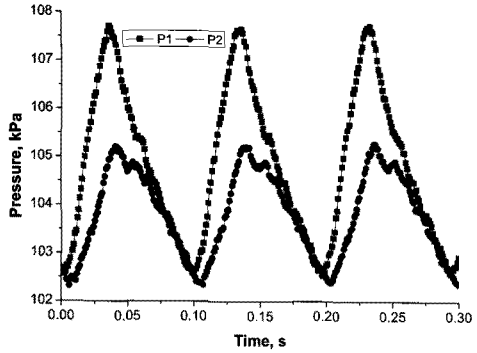

Fig. 8 Pressure wave at point 1 and point 2 for 48Hz motor speed

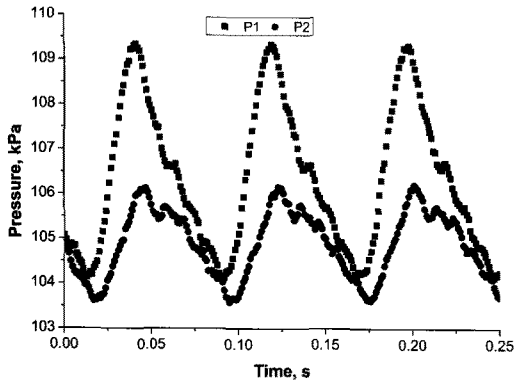

Fig. 9 Pressure wave at point 1 and point 2 for 60Hz motor speed

Table 2 contains the RMS AVG values of pressure in the 500mm straight, 60mm diameter bend 3 arm steel pipe corresponding to different motor speed for compression of air in reciprocating compressor. RMS pressure for point1 forms almost straight line as the motor speed increase from 12 Hz to 60 Hz it was similar pattern for point 2 but less in straight line slopes and values. At point 1, 101.90227, 102.8125, 103.6647, 104.9184, 106.4587kPa. RMS pressures were reported whereas the average pressures were 102.0752, 103.1227, 103.8523, 105.1430, 106.4587kPa against 101.7915, 102.4190, 102.9897, 103.8446, 104.9236kPa at point 2 as the motor run for 12, 24, 36, 48, 60 Hz, respectively. The average pressures were found at point 2 as 101.9228, 102.6076, 103.0170, 103.7975, 104.8535kPa. In the steel pipe the pressure loss due to its wall and passage and fluid flow phenomena were calculated as 0.1092, 0.3828, 0.6512, 1.0235, 1.4419% on RMS basis and 0.1493, 0.4995, 0.8043, 1.2797, 1.7507% for AVG for the different speeds of the compressor. It had a positive correlation with the compressor speed i.e. pressure loss increases with speed. Very small amount of percentages of RMS pressure loss were found in different compression speed for the both cases.

Table 2 Gas pressure loss through 3_arm steel pipe

Motor speed, Hz	P_in [RMS], kPa	P_in [AVG], kPa	P_out [RMS] kPa	P_out [AVG] kPa	Pressure loss on RMS(%)	Pressure loss on AVG(%)
12	101.9027	102.0752	101.7915	101.9228	0.1092	0.1493
24	102.8125	103.1227	102.4190	102.6076	0.3828	0.4995
36	103.6647	103.8523	102.9897	103.0170	0.6512	0.8043
48	104.9184	105.1430	103.8446	103.7975	1.0235	1.2797
60	106.4587	106.7218	104.9236	104.8535	1.4419	1.7507

The Against motor running for different speed, the fluctuation of pressures at different speed were calculated and summerized as in Table 3. There were 0.4982, 1.0596, 1.0837, 1.0132, 1.0118% amplitudes found in inlet and 0.3357, 0.7147, 0.7219, 0.5847, 0.4813% for outlet on the RMS basis. Then, the reduction of fluctuations were 0.1625, 0.3449, 0.3618, 0.4285 and 0.5305%at motor speed 12 Hz, 24 Hz, 36 Hz, 48, Hz and 60 Hz. On the basis of average of the pressure, amplitude reductions were reported as 0.1621, 0.3430, 0.3600,

0.4261, 0.5277% of average pressure for respective motor speed. It had increasing trends of amplitude reduction with speed of the motor for the both RMS and average basis. The measured pressure and simulated pressure were compared at point 1 and Point 2 (Fig. 10). There it is shown that the best match between them with little difference. The simulation unsteady pressure follows the route along with experimental of 107.7133, 107.6459, 107.7133 with 107.952, 108.056, 108.075kPa three maximum peaks of curve at point 1 and experimental pressure of 105.2131, 105.2054, 105.2743kPa with 104.689, 104.663, 104.686kPa three maximum CFD peaks for the curve at point 2. The three minimum values of pressure at point 1 for experiment and CFD (102.5877, 102.694), (102.6027, 102.754), (102.6925, 102.691), and at point 2 they were (102.3436, 102.306), (102.3895,102.330), (102.7262, 102.586). Because of best superimposing incident the two curves of experimental and simulation it can be concluded that the CFD simulated pressure can be accepted.

Table 3 Amplitude in gas flow through 3_arm steel pipe

Motor speed, Hz	Amplitude basis of RMS			Amplitude basis of AVG		
	Input, %	Output, %	Reduction (%)	Input, %	Output, %	Reduction (%)
12	0.4982	0.3357	0.1625	0.4974	0.3353	0.1621
24	1.0596	0.7147	0.3449	1.0564	0.7134	0.3430
36	1.0837	0.7219	0.3618	1.0818	0.7217	0.3600
48	1.0132	0.5847	0.4285	1.0110	0.5849	0.4261
60	1.0118	0.4813	0.5305	1.0093	0.4816	0.5277

The pressure amplitude values were calculated by FFT for input and output pressure passing through 3 arm curved steel pipe. In different motor speed, it were generated different amplitudes varying from 0.5077kPa to 1.0772kPa for inlet and it were no specific shape with initially increasing and then decreasing trends with motor speed. The outlet amplitudes also following same trends but with lesser values of 0.3470, 0.7320, 0.7435, 0.6071, 0.5050 kPa for 12 Hz to 60 Hz speed (Fig. 11).

The CFD analysis gives the pressure distribution inside the 3 arm steel pipe at entire time step of its unsteady situation cycle. Pressure simulation data at t= 0.032 s for 48Hz motor speed are presented as two end points P1, P2 and middle of the pipe as in the Fig. 12(a). It shows that for this time step maximum pressure 0.1045E+06Pa was at the inlet and it was declined as it advances through circular bend and reached at its lowest pressure at outlet point 2 with 0.1033E+06Pa. The pressure distribution is shown in colour map and numerical values for entire pipe. It can also explore the pressure situation in the bending part of the pipe where pressure measurement is difficult and erroneous.

Data collected from the simulation are presented by plotting them with time in Fig 13. For the first turn, the maximum and minimum pressure of a cycle were 108.075, 102.532kPa and at second turn, maximum 104.689kPa, minimum 102.306kPa pressure were obtained. The areal pressure distribution by its cross-section at first turn and second turn are as in the Fig. 12(b) and 12(c).

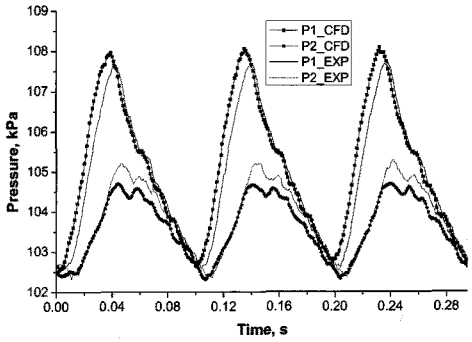

Fig. 10 Comparison of CFD simulation and experimental pressure at inlet and outlet

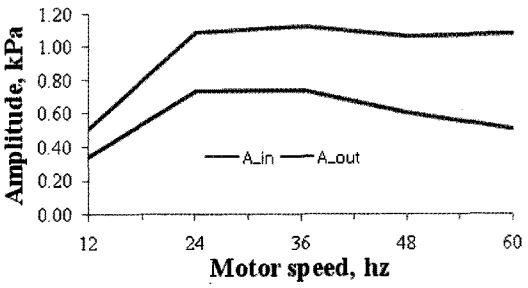

Fig. 11 Amplitude pressures at inlet and outlet

4. Conclusion

The pressure characteristics study of a bending steel pipe of 500mm length and 13mm diameter has explored by the both experimentally and numerically. The input amplitude found were 0.04982, 1.0596, 1.0837, 1.0132, 1.0118% at inlet and that of output amplitude were 0.3357, 0.7147, 0.7219, 0.5847, 0.4813% on RMS values for 12, 24, 36, 48, 60 Hz motor speed. The reduction of amplitude were 0.1625 ~ 0.5305% on RMS basis. The 0.1621 ~ 0.5277% amplitude were reduced on average basis. The RMS values of pressure at point 1 and point 2 were recorded as 101.9027 ~ 106.4587kPa and 102.0752 ~ 106.7218kPa. The percentage of pressure loss were 0.1092 ~ 1.4419% on RMS. In comparison to average, the losses were 0.1493% ~ 1.7507%. The pressure information which includes pulsation and pressure loss is very important in gas dealings section. Detail fluid flow phenomena inside the pipe at any point can be found from the numerical study. The wall pressure as well as central line pressure can also be determined.

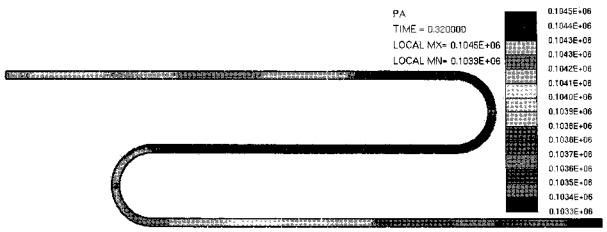

(a) Along length

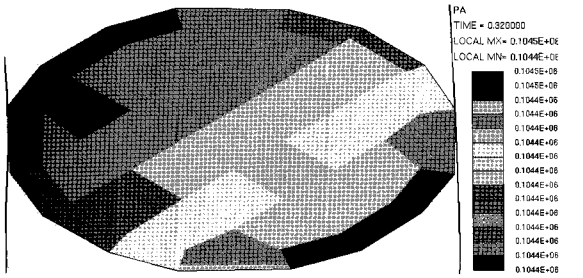

(b) First turn Cross-section

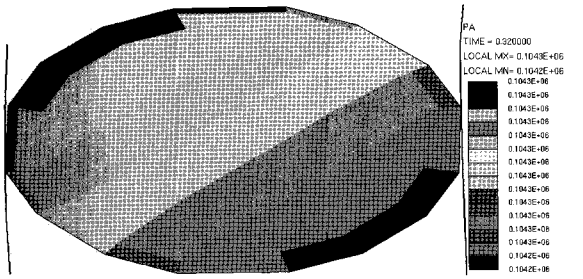

(c) Second turn Cross-section

Fig. 12 CFD simulated pressure distribution inside 3 arm steel pipe at 0.32s

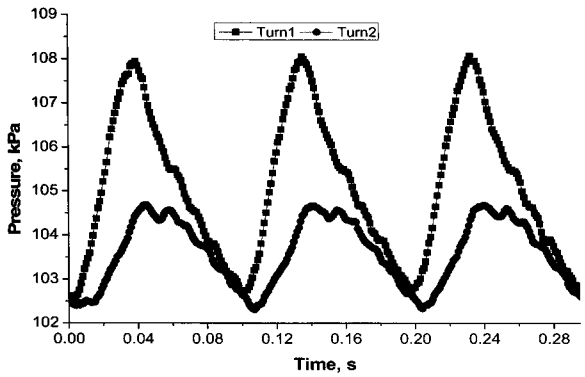

Fig. 13 Point pressure at Turn1 and Turn2

Acknowledgement

This research was financially supported by the Technology Innovation Project of Small and Medium Business Administration, Region Strategic Planning Project from Ministry of Knowledge Economy and Brain Korea 21 Project.

Reference

1. D. Das and T. N. Veziroglu, 2001, "Hydrogen production by biological process: a survey of literature 2001", Int. J. of Hydrogen Energy, Vol. 26, pp. 13~28.
2. T. N. Veziroglu, 1995, "Twenty years of the hydrogen movement", 1974-1994. Int. J. of Hydrogen Energy, Vol. 20, pp. 1~7.
3. C. J. Winter, 1987, Int. J. of Hydrogen Energy, Vol. 12, 521 INSPEC Compendex.
4. A. Midili and I. Dincer, 2007, "Key strategies of hydrogen energy systems for sustainability", Int J. of Hydrogen Energy, Vol. 32, pp. 511~524.
5. P. A. Okken, 1992, "Proceedings of the Ninth World Hydrogen Energy Conference. Paris (France)", p. 1723.

6. J. O. M. Bockris, 1981, "The economics of hydrogen as a fuel", Int J. of Hydrogen Energy", Vol. 6, pp. 223~241.
7. P. Forsberg and M. Karlstrom, 2007, "On optimal investment strategies for a hydrogen refueling station", Int J. of Hydrogen Energy, Vol. 32, pp. 647~660.
8. S. A. Heever and I. E. Grossman, 2003, "A strategy for the integration of production planning and reactive scheduling in the optimization of hydrogen supply network", Journal of Computers and Chemical Engineering, Vol. 27, pp. 1831~1839.
9. Origin Lab. Co., 2003, "Origin Reference v7.5", FFT Mathematical Description.
10. CD Adapco Group, 2004, "Methodology Star CD Version 3.24".